Lymphedema evaluation using noninvasive 3 Tesla magnetic resonance lymphangiography

Rachelle Crescenzi, PhD[1,#], **Paula MC Donahue, DPT**[2,3,#], **Kate Hartley, MD**[1], **Aditi A Desai, MD**[1], **Allison O. Scott, BA**[1], **Vaughn Braxton, MD**[1], **Helen Mahany, BA**[1], **Sarah K. Lants, BA**[1], and **Manus J. Donahue, PhD**[1,4,5,6,*]

[1]Radiology and Radiological Science, Vanderbilt University School of Medicine, Nashville, TN, USA

[2]Physical Medicine and Rehabilitation, Vanderbilt University School of Medicine, Nashville, TN, USA

[3]Dayani Center for Health and Wellness, Vanderbilt University School of Medicine, Nashville, TN, USA

[4]Neurology, Vanderbilt University School of Medicine, Nashville, TN, USA

[5]Psychiatry, Vanderbilt University School of Medicine, Nashville, TN, USA

[6]Physics and Astronomy, Vanderbilt University, Nashville, TN, USA

Abstract

Purpose—To exploit the long 3.0T relaxation times and low flow velocity of lymphatic fluid to develop a noninvasive 3.0T lymphangiography sequence and evaluate its relevance in patients with lymphedema.

Methods—A 3.0T turbo-spin-echo (TSE) pulse train with long echo time (TE$_{effective}$=600ms; shot-duration=13.2ms) and TSE-factor (TSE-factor=90) was developed and signal evolution simulated. The method was evaluated in healthy adults (n=11) and patients with unilateral breast cancer treatment-related lymphedema (BCRL; n=25), with a subgroup (n=5) of BCRL participants scanned before and after manual lymphatic drainage (MLD) therapy. Maximal lymphatic vessel cross-sectional area, signal-to-noise-ratio (SNR), and results from a five point categorical scoring system were recorded. Nonparametric tests were applied to evaluate study parameter differences between controls and patients, as well as between affected and contralateral sides in patients (significance criteria: two-sided $p<0.05$).

Results—Patient volunteers demonstrated larger lymphatic cross-sectional areas in the affected (arm=12.9±6.3mm^2; torso=17.2±15.6mm^2) vs. contralateral (arm=9.4±3.9mm^2; torso=9.1±4.6mm^2) side; this difference was significant both for the arm ($p=0.014$) and torso ($p=0.025$). Affected (arm: $p=0.010$; torso: $p=0.016$) but not contralateral (arm: $p=0.42$; torso: $p=0.71$) vessel areas were significantly elevated compared with control values. Lymphatic cross-

---

[*]**Corresponding author**: Manus J. Donahue, PhD, 1161 21st Avenue South, Vanderbilt University Institute of Imaging Science, Nashville, TN 37232, USA, Tel: +1 615.322.8350, Fax: +1 615.322.0734, mj.donahue@vanderbilt.edu.
[#]Authors contributed equally to this work

sectional areas reduced following MLD on the affected side (pre-MLD: arm=8.8±1.8mm^2; torso=31.4±26.0mm^2; post-MLD: arm=6.6±1.8mm^2; torso=23.1±24.3mm^2). This change was significant in the torso (p=0.036). The categorical scoring was found to be less specific for detecting lateralizing disease compared to lymphatic-vessel areas.

Conclusion—A 3.0T lymphangiography sequence is proposed, which allows for upper extremity lymph stasis to be detected in approximately 10 minutes without exogenous contrast agents.

Keywords

lymphangiography; lymphedema; MRI; manual lymphatic drainage; turbo spin echo; breast cancer

Introduction

The lymphatic system is a central component of the body's circulatory system, serving to (i) uptake plasma proteins and ultrafiltrate from blood capillaries, (ii) unidirectionally transport this lymphatic fluid through lymphatic vessels (i.e., lymphatics) by means of extrinsic contraction of tissue forces and intrinsic pumping of smooth muscle-lined lymphangions, (iii) process this fluid in lymphatic nodes, and (iv) return the majority of fluid (estimated three liters per day) back to the blood circulation via the lymphatic ducts and subclavian veins (1–4). As such, the lymphatic system is fundamental to maintaining tissue and plasma volume and osmolality homeostasis. Lymphatic vessels range in diameter from several nanometers (lymphatic capillaries) to 2–5 mm (larger collecting lymphatics), transport lymphatic fluid at a comparatively slow velocity (<1 mm/s), and are present systemically (5–8).

The lymphatic nodes and vessels are the primary route for cancer metastasis, and lymphatic dysfunction has been implicated in a variety of debilitating conditions including lymphedema, hypertension, obesity, infection, and fat disorders (2,4,9,10). Most recently, lymphatics within the central nervous system (CNS) have been observed (11,12), which may have direct relevance for diseases of the CNS with unknown etiology, including multiple sclerosis and Alzheimer's disease (13). The relevance of improving our understanding of lymphatic functioning has been the topic of multiple recent review articles (2,14,15), yet one barrier to addressing this fully is the lack of imaging methods that can be applied routinely to characterize lymphatic transport.

E*x vivo* (16) and *in vivo* (17) MR imaging work has demonstrated abilities to visualize lymphatic nodes directly at high spatial resolution. Methods proven successful for evaluating tissue health in the brain and other organs are capable of quantifying tissue environment in terms of chemical profile (17) and perfusion (7) and have been applied to the lymphatic system to show discriminatory capacity for lymphatic dysfunction. The relevance of directly visualizing lymphatic vessels using either x-ray fluoroscopy or paramagnetic contrast agents with MR has also been recognized, and there are a growing number of clinical implementations of these methods (18). While these methods have emerged as important tools for visualizing lymphatic flow, including backflow and alternative routes for understanding individual clinical presentation and treatment, existing lymphangiography methods have limitations. Specifically, these methods require injection of exogenous

contrast agents and tracking these agents as they are taken up by lymphatic capillaries and transported by larger lymphatic collectors, which occurs at a low velocity of < 1 mm/s (7,8). Thus, these methods generally require 45–90 min of imaging time, and it remains unclear how exogenous contrast agents influence lymphatic transport. Performing these methods longitudinally or in response to interventions is frequently impractical owing to time, dose restrictions, and reliability of repeated delivery.

Recently, relaxation time measurements of water in human lymphatic fluid and tissue have been reported, along with ranges of flow velocities and vessel sizes (7). This information provides a foundation for developing MRI methods that can directly visualize the lymphatic architecture, and in turn quantify adjustments in lymphatic collector structure in disease. Two elegant studies have utilized estimated lymphatic relaxation times in pelvis and lower extremities to perform lymphangiography of large lymphatic collectors at a field strength of 1.5 Tesla (19,20), and it has been shown that such contrast correlates with reference-standard methods that require exogenous agents. The purpose of this study is to utilize this recent information to outline a noninvasive 3.0 Tesla (3.0T) lymphangiography method, to quantify normative ranges of signal-to-noise ratio (SNR) and imaging characteristics in healthy adults, and to evaluate the ability of this method to detect lymph stasis in patients with breast cancer treatment-related lymphedema (BCRL).

Materials and Methods

Volunteer demographics

All volunteers (n=36; gender=female; handedness=right) provided informed, written consent in accordance with the local Institutional Review Board. To evaluate potential differences between patient and control volunteers, patients with BCRL (age range=44–80 years; mean age=62 years; Stage=0–2) and healthy gender and age-matched controls within approximately one decade of life (n=11; age range=33–68 years; mean age=50 years) were included. Patients consisted of sub-clinical BCRL Stage 0 (n=14; age range=44–74 years; mean age=61 years) and symptomatic BCRL Stage 1–2 (n=11; age range=46–80 years; mean age=63 years).

A secondary aim was to evaluate whether lymph stasis decreased following a single session of manual lymphatic drainage (MLD) therapy. For this supplemental aim we evaluated a separate cohort of patients (n=5; age range=64–81 years; mean age=70 years) who were imaged before and immediately after MLD therapy. Note that the MLD component of the study was intended only to evaluate whether lymphatic collector contrast changed in an expected manner before and after MLD. Information regarding lymphedema stage, time since lymph node dissection, and lymphedema location were determined by a Lymphology Association of North America (LANA)-certified physical therapist (*PMCD*).

Acquisition

All volunteers were scanned at 3.0T (Philips Healthcare, Best, The Netherlands) using body coil radiofrequency transmission and a 16-channel torso coil for reception. First structural imaging, consisting of diffusion weighted imaging with background suppression (DWIBS)

(21), T_2-weighted, and T_1-weighted imaging of the axillary nodes, was performed to identify axillary lymphatic node locations using previously reported imaging parameters (17). Relevant scan parameters were:

> DWIBS: inversion recovery spin echo; TR/TE/TI=7558/54/260 ms; field-of-view = 445×241×192 mm^3, spatial resolution=3×3×5 mm^3; b-value=800 s/mm^2, SENSE-factor=2, averages=7, duration=3 min.

> T_1-weighted mDIXON imaging: 3D gradient echo, TR/TE$_1$/TE$_2$=3.5/1.16/2.20 ms, field-of-view=520×424×202 mm^3, spatial resolution=0.9×0.9×2.5 mm^3, SENSE-factor=1.9, duration=21s.

> T_2-weighted structural imaging: 2D multi-shot turbo spin echo (TSE-factor=12), TE=60 ms, field-of-view=180×162×50 mm^3, spatial resolution=0.5×0.5×5 mm^3, refocusing angle=120 degrees, SPAIR fat suppression.

The novel 3.0T lymphangiography sequence was performed using the following scan parameters: 3D TSE, TR/TE=3000/600 ms, TSE-factor=90, field-of-view=445×241×180 mm^3, spatial resolution=1.39 ×1.39×3 mm^3, oversampling=120 mm (A/P direction), two 60 mm thick pre-saturation slabs placed 20 mm inferior and superior to imaging volume, SPIR fat suppression at 190 Hz, averages=2, k-space ordering=linear cartesian; duration=10 min 51s. A schematic of this sequence is shown in Figure 1A. A supplementary discussion of the theory is included in Supporting Information document.

Manual lymphatic drainage (MLD) intervention

In a subgroup of volunteers (n=7), the imaging protocol was repeated immediately following a 50-minute session of MLD that was performed by the same certified lymphedema physical therapist. The MLD session consisted of stimulating the bilateral supraclavicular fossae, cervical lymphatic nodes, shoulder collectors and axillary lymphatic nodes, along with stimulating anterior and posterior axillo-axillary pathways, ipsilateral inguinal lymphatic nodes and axillo-inguinal pathway, deep abdominals, involved quadrant and arm applying stretch to the tissues proximal to distal toward the direction of intended lymphatic flow with temporary redirection towards uninvolved orthogonal truncal quadrants and involved posterior shoulder (22).

Analysis

The analysis was divided into a quantitative assessment of fractional lymphatic signal, SNR, and maximal lymphatic vessel cross-sectional area as well as a categorical scoring of the lymphatic angiography sequence by two raters. All quantitative measurements were recorded from orthogonal magnitude image reconstructions of the lymphangiography scan, and the five point categorical scoring was performed on a 3D maximum-intensity-projection (MIP) of the lymphangiography scan.

Lymphatic signal: Fractional lymphatic signal (S/S_0) was calculated by choosing the largest discernable lymphatic vessel on the lymphangiography scan, separately in the arm and torso. The signal was normalized by the equilibrium signal (S_0), which was calculated from the measured CSF signal (discernable from the thoracic segment of the spinal cord) and scaled

to equilibrium using an identical equation presented in the literature (23) and using the previously published water density of CSF of 1 ml water/ml CSF (24), along with TR=3000 ms, $T_{1,CSF}$=4300 ms (25), TE=600 ms, and $T_{2,CSF}$=1442 ms (26). The evolution of the signal is also shown for these parameters in Figure 1B.

Lymphatic fluid SNR: In the same regions as described above, the lymphatic signal was normalized by a noise measurement taken from an identical volume in all subjects and SNR was recorded.

Lymphatic vessel size: In the same regions, the cross-sectional areas of the lymphatic vessels were recorded. These measurements were taken at the maximum discernable diameter of the lymphatic vessels in the axial imaging plane in both control and patient volunteers, noting that larger diameters may be representative of lymph stasis or vessel impairment. This procedure is analogous to procedures for grading stenosis degree on blood angiography images. Care was taken to avoid extravascular, (subcutaneous) edema, pleural effusion, glenohumeral joint effusion, fluid within the long head biceps tendon sheath, and other fluid not localized to lymphatics. Lymphatic vessels had to be continuous through multiple slices in orthogonal reconstructions; the images were re-sliced perpendicular to the lymphatic vessel on the sagittal and coronal representations and drawn on the axial image.

Radiological scoring: Two raters also evaluated a 3D MIP of the lymphangiography scan using the scoring system proposed in Table 1. The scoring system is intended to reflect contrast consistent with increasing levels of lymphatic stasis and vessel tortuosity, as hypothesized responses to mechanical insufficiency induced by lymph node removal. The raters consisted of two clinical readers, both faculty radiologists at our institution (*KH and AAD*), one with subspecialty training in musculoskeletal radiology and one with subspecialty training in breast radiology. Rating was performed independently and a consensus score was determined by agreement when individual scores were discordant.

Statistical considerations

The objectives of this study were to quantify the normative ranges of lymphatic fluid signal and SNR, lymphatic vessel diameter, and radiological scoring in patients with BCRL and age-matched female controls, as well as to evaluate whether these parameters were discriminatory for lymphedema. A secondary objective was to physically modulate the distribution of lymphatic fluid in the upper extremities and quadrants using MLD therapy and evaluate whether lymphangiography contrast decreased in the affected arm and torso of patients immediately following the intervention.

Descriptive statistics, including means, standard deviations, and ranges for continuous parameters were calculated. Investigations for outliers (2.5 standard deviations from the mean) were made. To test the difference in study parameters between controls and patients with BCRL, the Wilcoxon rank-sum test was applied. To evaluate differences in study parameters before and after MLD, as well as between left and right sides, the matched Wilcoxon signed-rank test was applied. In all cases, a corrected *p*-value<0.05 was required for significance. Due to the small sample size in the MLD component of the study, an effect size was also calculated (Cohen's *d*). Cohen's kappa was calculated to evaluate inter-rater

agreement in the scoring system with agreement classifications defined using previously reported agreement criteria (27) for Cohen's kappa = 0.21–0.40 (fair), 0.41–0.60 (moderate), 0.61–0.80 (substantial), 0.81–1.00 (perfect).

Results

The proposed lymphangiography pulse sequence along with simulated signal is shown in Figure 1A,B. The middle of the echo train occurs when the lymphatic fluid signal is approximately 16% of the equilibrium signal S_0 and blood and muscle signal are null. The measured SNR was 13.4±5.6 and 10.4±4.2 in control arm and torso, respectively, and did not differ significantly between left and right ($p=0.70$) or between arm and torso ($p=0.067$). The measured fractional lymphatic signal (S/S_0) was 9.8±4.4%. Structural imaging in a control volunteer is shown below in Figure 1C–G, and depicts the location of axillary lymphatic nodes over which the lymphangiography scan was planned, along with a reconstructed MIP of the lymphangiography scan. Note that since lymphatic node T_1 and T_2 are substantially lower than lymphatic fluid T_1 and T_2, the lymphatic nodes are not clearly visible in the lymphangiography sequence. For completeness, results from the high spatial resolution structural imaging are also shown highlighting the approximate location and depth of the axillary lymphatic nodes.

In control volunteers, lymphatic vessel cross-sectional area measurements were not found to be significantly different when considering the arm ($p=0.76$; left=8.8±4.2 mm^2; right=8.4±1.6 mm^2) or torso ($p=0.97$; left=8.7±2.1 mm^2; right=8.7±2.8 mm^2) regions, nor did the arm or torso cross-sectional areas differ significantly between subjects ($p=0.85$). An example of the cross-sectional area measurement procedure is shown in Figure 2. By contrast, patient volunteers demonstrated larger cross-sectional area diameters in the affected (arm=12.9±6.3 mm^2; torso=17.2±15.6 mm^2) vs. contralateral (arm = 9.4±3.9 mm^2; torso=9.1±4.6 mm^2) side; this difference was significant both for the arm ($p=0.014$) and torso ($p=0.025$). Furthermore, when compared with control values, the patients' affected (arm: $p=0.010$; torso: $p=0.016$) values were significantly elevated, whereas patients' contralateral (arm: $p=0.42$; torso: $p=0.71$) values were not elevated compared to control values. The same significant relationships were observed when patients were stratified as to those with sub-clinical lymphedema (i.e., Stage 0) vs. those with symptomatic (i.e., overt swelling) lymphedema Stages 1–2. All values are summarized in Table 2, and a lymphangiography scan from a representative patient is shown in Figure 3.

Next, data were considered using the categorical scoring system rather than the quantitative cross-sectional area measurements. Moderate agreement was found between the two independent raters (Cohen's kappa=0.50; confidence interval=0.35–0.64) with an agreement due to true concordance (observed agreement – random agreement) of 0.36. The lymphatic duct was visible in 100% of control volunteers and 88% of patient volunteers. Lymphangiography scans were considered of acceptable quality in 100% of controls and 92% (23 / 25) of patients with BCRL. Unacceptable quality in the two cases was attributable to an artifact from sternal wires in one case and a large motion artifact in the other. Consensus scores from both raters are summarized in Table 2. Scores did not differ significantly between left and right sides in control volunteers ($p=1.0$; left=1.9±0.8;

right=1.9±0.8); the scores also did not differ significantly between affected and contralateral sides considering all BCRL patient volunteers (*p*=0.82; affected=2.1±1.3; contralateral=2.2±1.3). However, when only patients with symptomatic Stages 1–2 BCRL were considered, the categorical score was higher (*p*=0.048) in the affected side (score=2.7±1.5) compared to control volunteer scores, but not compared to contralateral scores in the same patients (*p*=0.22). These findings are consistent with the categorical scoring system having moderate agreement between independent raters, but having potential specificity for distinguishing healthy from diseased conditions primarily in symptomatic patients.

Finally, in the subgroup of patients scanned before and after MLD, maximal lymphatic cross-sectional area was observed to reduce on the affected side (pre-MLD: arm=8.8±1.8 mm^2; torso=31.4±26.0 mm^2 vs. post-MLD: arm=6.6±1.8 mm^2; torso=23.1±24.3 mm^2). This change was significant in the torso region (*p*=0.036) and just beyond criteria for significance in the arm region (*p*=0.054). No change was observed before vs. after MLD in the contralateral regions (pre-MLD: arm=10.7±5.3 mm^2; torso=9.0±2.9 mm^2 vs. post-MLD: arm=10.6±5.1 mm^2; torso=8.1±3.8 mm^2) for either arm (*p*=0.97) or torso (*p*=0.71). Before MLD, the categorical scores were 4.2±0.4 and 2.0±0.7 on the affected and contralateral side, respectively. After MLD, the scores were 3.6±0.9 and 1.6±0.5 on the affected and contralateral side respectively. These changes did not meet statistical criteria for significance on either the affected (*p*=0.37) or contralateral (*p*=0.18) sides, however the effect sizes were large on both the affected (Cohen's *d*=0.81) and contralateral (Cohen's *d*=0.63) side. An example of a patient scanned before and immediately after MLD is shown in Figure 4.

Figure 5 summarizes the group-level results.

Discussion

We utilized recently-measured 3.0T MRI relaxation times of lymphatic fluid and known ranges of lymphatic and blood flow velocities to propose a noninvasive 3.0T lymphangiography pulse sequence. The sensitivity of the sequence to lymphatic fluid, relative to blood, was first investigated through simulations, after which normative ranges of SNR were calculated in healthy adult female participants. Maximal lymphatic collector cross-sectional area was calculated in healthy participants and patients with known lymphatic compromise, as a potential quantitative measure of lymph stasis. A categorical radiologic scoring system was also devised based on lymphangiograms from patients with BCRL. The primary findings are that maximal lymphatic cross-sectional area was elevated on the affected side of patients with BCRL relative to the contralateral side and control values. The five point categorical scoring system provided elevated scores on the affected side of advanced stage patients only, indicating that the scoring system (categorical variable) is less sensitive to lateralizing BCRL pathology than the continuous variable of lymphatic vessel measurements.

A concern while developing this protocol was that blood and lymphatic vessels appear very similar in maximum-intensity-projection reconstructions, and these vessels are often in close proximity such that distinguishing between the two can be difficult. In anticipation of this,

we implemented several procedures for ensuring that blood-water signal was suppressed. First, we utilized a long echo time sequence ($TE_{effective}$=600 ms; $TE_{equivalent}$=491 ms). While 3.0T lymphatic T_2 is approximately 610 ms (7), 3.0T venous and arterial blood-water T_2 are less than 50 ms and 150 ms, respectively, including microvessels with a hematocrit < 0.30 (28). Therefore, residual blood-water signal is << 1% for the majority of the readout. Additionally, we incorporated a long TSE pulse train (TSE-factor=90; shot duration=1187 ms), which serves to inefficiently refocus fast-flowing spins, as is the case for blood-water. Finally, the possibility of inflow of fresh blood-water was a concern, and to reduce this we implemented broad spatially selective excitation pulses with dephasing gradients above and below the imaging volume. We calculated the magnetization in the hypothesized lymphatic vessels and found that the signal was similar to the estimated signal from the Bloch equation simulations for lymphatic fluid, however slightly reduced potentially due to partial volume effects at our spatial resolution. The simulated blood-water signal was less than 1% by the center of the echo train.

Lymphatic vessels are generally reported to be 2–5 mm in diameter (for large vessels such as the thoracic trunk) ranging down to several nanometers for smaller vessels (5). Our spatial resolution (in-plane=1.39×1.39 mm^2) allowed for quantification of only larger lymphatic collectors (minimal cross-sectional diameter of approximately 1–2 mm). In healthy subjects, we found the largest lymphatic arm and torso collectors to have a cross-sectional area of approximately 8–9 mm^2, with corresponding diameter of approximately 3–3.4 mm. This is approximately consistent with expected sizes for larger lymphatic vessels in these regions, which have been suggested to fluctuate in diameter from 2–4 mm for a lymphatic fluid flow of 1–3 ml/min and pressure of 1.5 mmHg (29).

The refocusing pulse train used in this study utilized a constant refocusing angle of 110 degrees and startup dummy echoes in which no data were acquired to reduce signal instability for early refocusing pulses. This strategy was implemented to reduce specific-absorption-ratio (SAR) while still maintaining adequate lymphatic signal across the TSE pulse train. We additionally investigated variable refocusing angles (e.g., combinations of refocusing sweep ranges from 10 to 180 degrees) as have been summarized in the literature for separate applications (23,30). While it is possible to slightly reduce the decay of the lymphatic signal across the readout with different sweep parameters, this comes at the cost of also increasing the residual blood-water signal. However, future studies which experimentally investigate the effect of the refocusing pulse train properties on blood and lymphatic fluid signal could be important for improving SNR and narrowing the lymphatic fluid point spread function. Additional suppression of blood-water spin isochromats could be achieved using principles of velocity-induced phase suppression and delay alternating with nutation for tailored excitation (DANTE) modules, which have been successful in suppressing both slow blood flow near the perimeter of vessels as well as slow CSF flow in intracranial vessel wall imaging applications (31–33). DANTE modules could be implemented in conjunction with lower TSE-factors and shorter echo times to improve SNR, however this has not yet been investigated.

Both lymphatic fluid (flow velocity = 0.3–1 mm/s; T_1/T_2=3100/610 ms) (7,34) and CSF (flow velocity=10–15 mm/s in lumbar and cervical spine; T_1/T_2=4300/1442 ms) (25,35)

have flow velocities that are low, and relaxation times that are long, compared to blood (28,36). Therefore, CSF signal is also expected to appear bright in the proposed lymphagiography sequence, as demonstrated by the simulations presented here and the case examples. Since CSF is localized to the spinal cord, this was not a major concern, and CSF regions can easily be cropped out of orthogonal MIP representations as is frequently performed for intracranial blood time-of-flight MR angiography reconstructions. Other applications of the lymphangiography sequence to cervical lymphatic vessels or nodes, or to applications in the central nervous system, may benefit from different reconstruction and acquisition parameters that desensitize the sequence to CSF.

Noninvasive lymphangiography techniques could have broad relevance, both in research studies for investigating onset and mechanisms of lymphatic compromise as well as in a clinical setting as part of screening protocols. In the research setting, lymph stasis and altered vessel structure are well-known effects of lymphatic dysfunction, especially following breast cancer where secondary lymphedema occurs in approximately 30% of breast cancer survivors experiencing lymph node dissection and radiation therapy (37). Lower extremity lymphedema has a conservative reported prevalence of 10–36% in patients undergoing gynecological or prostate cancer therapies including sentinel node biopsy, and 12–64% in patients undergoing aggressive dissection for melanoma cancer (38,39). Therapy management, including MLD as a component of complete decompression therapy, has generally not been optimized. Controversy remains as to how MLD impacts lymphatic functioning and if so, then for what duration and for which individual. Noninvasive biomarkers of lymphatic flow and lymphatic vessel cross-sectional area could therefore serve as end points in longitudinal trials of therapy optimization, and in particular enable detection of intact pathways for clearance in a patient-specific manner.

The radiological five point scoring system proposed here was based on expected changes in lymphatic fluid accumulation as a function of increasing lymphedema stage, and therefore is based on physiological expectations rather than rigorous evaluation of correspondence between imaging findings and prognosis or diagnosis. Results are consistent with the lymphangiography sequence detecting quantitative changes in maximal lymphatic vessel area immediately after MLD, however assessing change in lymph stasis is less clear when only using the categorical grading system. It was observed that while the extent of contrast consistent with lymph stasis reduced following MLD, as evidenced by the cross-sectional area scores, the overall category of the image did not shift on general. Otherwise stated, a patient may exhibit the same general pattern of contrast for the same score, just the extent of pattern may be lower. The current study was powered to demonstrate expected differences in lymphangiography contrast between patient and control volunteers; however future work in a larger cohort would benefit from rigorously evaluating the sensitivity of this scoring system and refining the categories where appropriate, and finally by internally validating the calibration and discrimination using the bootstrap to estimate the model's likely performance on a new sample of subjects from the same patient stream.

The non-contrast lymphangiography method was shown to provide visualization of lymphatic vessel dysfunction consistent with lymph stasis and/or lymphatic structural impairment in patients with unilateral BCRL. These findings warrant further investigation of

the varying degrees of lymphatic vessel dysfunction and the relationship to condition severity as well as response to therapies intended to optimize and/or restore lymphatic pumping. In the given patient cohort, the mechanism causing lymphatic impairment is thought to be a condition of impaired pumping brought on by a mechanical insufficiency after axillary lymphatic node removal. MR lymphangiography may have the potential to evaluate the degree of lymphatic fluid reflux and lymphatic network response to the known insults from cancer therapies, as well as investigate structure dysfunction in cases of primary lymphedema with unknown causes. Understanding the degree and involvement of lymphatic dysfunction would likely inform the most effective prevention and management therapies for lymphedema and provide a more sensitive means of precision medicine through periodic surveillance of an individual's lymphatics. For example, with our noted patient example pre- and post-MLD session, her post-MLD lymphangiography indicates a specific need for future MLD sessions to focus attention on rerouting the remaining congestion along the upper lateral chest wall to the ipsilateral lower quadrant following her visualized lymphatic collector pathways. Additionally, there is also an opportunity for lymphangiography to inform a patient's individual risk of developing secondary lymphedema through pre- treatment evaluation of their intact and otherwise assumed healthy lymphatic system, which may provide researchers and clinicians with a new prognostic measure indicative of higher predisposition for secondary lymphedema given premorbid status.

The findings should also be considered in the context of several limitations. First, the sample size utilized (n=36), including 11 control and 25 BCRL patients, is too small to allow for clinical questions regarding lymph stasis to be rigorously addressed, and rather was intended to investigate the ability of the proposed method to identify lymph stasis only in the first instance. Future work with a larger cohort spanning more anatomical regions and representing more primary and secondary lymphedema stages is warranted to investigate clinically-relevant questions. Second, the spatial resolution employed here was not sufficient to allow for lymphatic collectors with a cross-sectional area less than approximately 2 mm^2 to be depicted, and therefore this method is primarily sensitive to lymphatic stasis present in patients with lymphedema where vessels appear engorged. Future work should focus on improving the spatial resolution, which could be accomplished by lowering the TSE shot number and reducing the field-of-view to focus on a more confined region of interest. It is likely that the measured lymphatic signal was underestimated slightly relative to simulation due to partial volume effects between the perimeter of the vessel and surrounding tissues. Third, no independent reference standard was utilized in this study. The standard for lymphangiography remains x-ray fluoroscopy, and co-registering such lymphangiograms, which are necessarily acquired in separate scan sessions and locations, is not straightforward. Future work that utilizes Gd-based lymphangiography, which can be performed in approximately 60 min and in the same scan session as the proposed noninvasive lymphangiography scan, would be a logical extension to better validate this sequence and is being pursued in ongoing investigations.

In conclusion, we demonstrate for the first time abilities to perform 3.0T lymphangiography of the upper body noninvasively using turbo-spin-echo MR pulse sequences. Contrast consistent with lateralizing disease was observed in patients with known secondary lymphedema from breast cancer treatment-related lymphedema, which also adjusted in an

Author Manuscript

expected manner following manipulation of lymph stasis through manual lymphatic drainage therapy. These findings suggest that MR has potential to evaluate lymphatic functioning and lymphedema treatment response, and may have relevance for informing personalized lymphedema risk and precision-treatment.

Supplementary Material

Refer to Web version on PubMed Central for supplementary material.

Acknowledgments

References

1. Aukland K, Reed RK. Interstitial-lymphatic mechanisms in the control of extracellular fluid volume. Physiological reviews. 1993; 73(1):1–78. [PubMed: 8419962]

2. Mortimer PS, Rockson SG. New developments in clinical aspects of lymphatic disease. The Journal of clinical investigation. 2014; 124(3):915–921. [PubMed: 24590276]

3. Swartz MA. The physiology of the lymphatic system. Advanced drug delivery reviews. 2001; 50(1–2):3–20. [PubMed: 11489331]

4. Titze J. Interstitial fluid homeostasis and pressure: news from the black box. Kidney international. 2013; 84(5):869–871. [PubMed: 24172732]

5. Ruddle NH. Lymphatic vessels and tertiary lymphoid organs. The Journal of clinical investigation. 2014; 124(3):953–959. [PubMed: 24590281]

6. Stranford S, Ruddle NH. Follicular dendritic cells, conduits, lymphatic vessels, and high endothelial venules in tertiary lymphoid organs: Parallels with lymph node stroma. Frontiers in immunology. 2012; 3:350. [PubMed: 23230435]

7. Rane S, Donahue PM, Towse T, et al. Clinical feasibility of noninvasive visualization of lymphatic flow with principles of spin labeling MR imaging: implications for lymphedema assessment. Radiology. 2013; 269(3):893–902. [PubMed: 23864103]

8. Modi S, Stanton AW, Svensson WE, Peters AM, Mortimer PS, Levick JR. Human lymphatic pumping measured in healthy and lymphoedematous arms by lymphatic congestion lymphoscintigraphy. The Journal of physiology. 2007; 583(Pt 1):271–285. [PubMed: 17569739]

9. Karaman S, Detmar M. Mechanisms of lymphatic metastasis. The Journal of clinical investigation. 2014; 124(3):922–928. [PubMed: 24590277]

10. Radhakrishnan K, Rockson SG. The clinical spectrum of lymphatic disease. Annals of the New York Academy of Sciences. 2008; 1131:155–184. [PubMed: 18519969]

11. Louveau A, Smirnov I, Keyes TJ, et al. Structural and functional features of central nervous system lymphatic vessels. Nature. 2015; 523(7560):337–341. [PubMed: 26030524]

12. Aspelund A, Antila S, Proulx ST, et al. A dural lymphatic vascular system that drains brain interstitial fluid and macromolecules. The Journal of experimental medicine. 2015; 212(7):991–999. [PubMed: 26077718]

13. Bradstreet JJ, Ruggiero M, Pacini S. Commentary: Structural and functional features of central nervous system lymphatic vessels. Frontiers in neuroscience. 2015; 9:485. [PubMed: 26733797]

14. Titze J, Machnik A. Sodium sensing in the interstitium and relationship to hypertension. Curr Opin Nephrol Hypertens. 2010; 19(4):385–392. [PubMed: 20571401]

15. Welsh JD, Kahn ML, Sweet DT. Lymphovenous hemostasis and the role of platelets in regulating lymphatic flow and lymphatic vessel maturation. Blood. 2016; 128(9):1169–1173. [PubMed: 27385789]

16. Korteweg MA, Zwanenburg JJ, Hoogduin JM, et al. Dissected sentinel lymph nodes of breast cancer patients: characterization with high-spatial-resolution 7-T MR imaging. Radiology. 2011; 261(1):127–135. [PubMed: 21673230]

17. Donahue MJ, Donahue PC, Rane S, et al. Assessment of lymphatic impairment and interstitial protein accumulation in patients with breast cancer treatment-related lymphedema using CEST MRI. Magn Reson Med. 2016; 75(1):345–355. [PubMed: 25752499]

18. Lucarelli RT, Ogawa M, Kosaka N, Turkbey B, Kobayashi H, Choyke PL. New approaches to lymphatic imaging. Lymphatic research and biology. 2009; 7(4):205–214. [PubMed: 20143919]

19. Arrive L, Azizi L, Lewin M, et al. MR lymphography of abdominal and retroperitoneal lymphatic vessels. AJR Am J Roentgenol. 2007; 189(5):1051–1058. [PubMed: 17954639]

20. Lohrmann C, Foeldi E, Langer M. Diffuse lymphangiomatosis with genital involvement-- evaluation with magnetic resonance lymphangiography. Urol Oncol. 2011; 29(5):515–522. [PubMed: 19914101]

21. Kwee TC, Takahara T, Ochiai R, Nievelstein RA, Luijten PR. Diffusion-weighted whole-body imaging with background body signal suppression (DWIBS): features and potential applications in oncology. European radiology. 2008; 18(9):1937–1952. [PubMed: 18446344]

22. Zuther, JE. Lymphedema Management: the comprehensive guide for practitioners. Stuttgart, Germany: Thieme; 2009.

23. Busse RF, Hariharan H, Vu A, Brittain JH. Fast spin echo sequences with very long echo trains: design of variable refocusing flip angle schedules and generation of clinical T2 contrast. Magnetic resonance in medicine. 2006; 55(5):1030–1037. [PubMed: 16598719]

24. Donahue MJ, Lu H, Jones CK, Edden RA, Pekar JJ, van Zijl PC. Theoretical and experimental investigation of the VASO contrast mechanism. Magnetic resonance in medicine. 2006; 56(6): 1261–1273. [PubMed: 17075857]

25. Lu H, Nagae-Poetscher LM, Golay X, Lin D, Pomper M, van Zijl PC. Routine clinical brain MRI sequences for use at 3.0 Tesla. Journal of magnetic resonance imaging : JMRI. 2005; 22(1):13–22. [PubMed: 15971174]

26. Donahue MJ, Juttukonda MR, Watchmaker JM. Noise concerns and post-processing procedures in cerebral blood flow (CBF) and cerebral blood volume (CBV) functional magnetic resonance imaging. NeuroImage. 2016 [Epub ahead of print].

27. Landis JR, Koch GG. The measurement of observer agreement for categorical data. Biometrics. 1977; 33(1):159–174. [PubMed: 843571]

28. Zhao JM, Clingman CS, Narvainen MJ, Kauppinen RA, van Zijl PC. Oxygenation and hematocrit dependence of transverse relaxation rates of blood at 3T. Magnetic resonance in medicine. 2007; 58(3):592–597. [PubMed: 17763354]

29. Quick CM, Venugopal AM, Gashev AA, Zawieja DC, Stewart RH. Intrinsic pump-conduit behavior of lymphangions. American journal of physiology Regulatory, integrative and comparative physiology. 2007; 292(4):R1510–R1518.

30. Dieleman N, Yang W, Abrigo JM, et al. Magnetic Resonance Imaging of Plaque Morphology, Burden, and Distribution in Patients With Symptomatic Middle Cerebral Artery Stenosis. Stroke; a journal of cerebral circulation. 2016; 47(7):1797–1802.

31. Li L, Miller KL, Jezzard P. DANTE-prepared pulse trains: a novel approach to motion-sensitized and motion-suppressed quantitative magnetic resonance imaging. Magnetic resonance in medicine. 2012; 68(5):1423–1438. [PubMed: 22246917]

32. Morris GA, Freeman R. Selective excitation in Fourier transform nuclear magnetic resonance. 1978. Journal of magnetic resonance. 2011; 213(2):214–243. [PubMed: 22152346]

33. Mosher TJ, Smith MB. A DANTE tagging sequence for the evaluation of translational sample motion. Magnetic resonance in medicine. 1990; 15(2):334–339. [PubMed: 2392056]

34. Kwon S, Sevick-Muraca EM. Noninvasive quantitative imaging of lymph function in mice. Lymphat Res Biol. 2007; 5(4):219–231. [PubMed: 18370912]

35. Enzmann DR, Pelc NJ. Normal flow patterns of intracranial and spinal cerebrospinal fluid defined with phase-contrast cine MR imaging. Radiology. 1991; 178(2):467–474. [PubMed: 1987610]

36. Piechnik SK, Chiarelli PA, Jezzard P. Modelling vascular reactivity to investigate the basis of the relationship between cerebral blood volume and flow under CO2 manipulation. NeuroImage. 2008; 39(1):107–118. [PubMed: 17920935]

37. DiSipio T, Rye S, Newman B, Hayes S. Incidence of unilateral arm lymphoedema after breast cancer: a systematic review and meta-analysis. Lancet Oncol. 2013; 14(6):500–515. [PubMed: 23540561]

38. Beesley V, Janda M, Eakin E, Obermair A, Battistutta D. Lymphedema after gynecological cancer treatment : prevalence, correlates, and supportive care needs. Cancer. 2007; 109(12):2607–2614. [PubMed: 17474128]

39. Cosgriff N, Gordon S. Cancer-related lymphoedema in males: a literature review. Journal of Lymphoedema. 2010; 5(2):49–61.
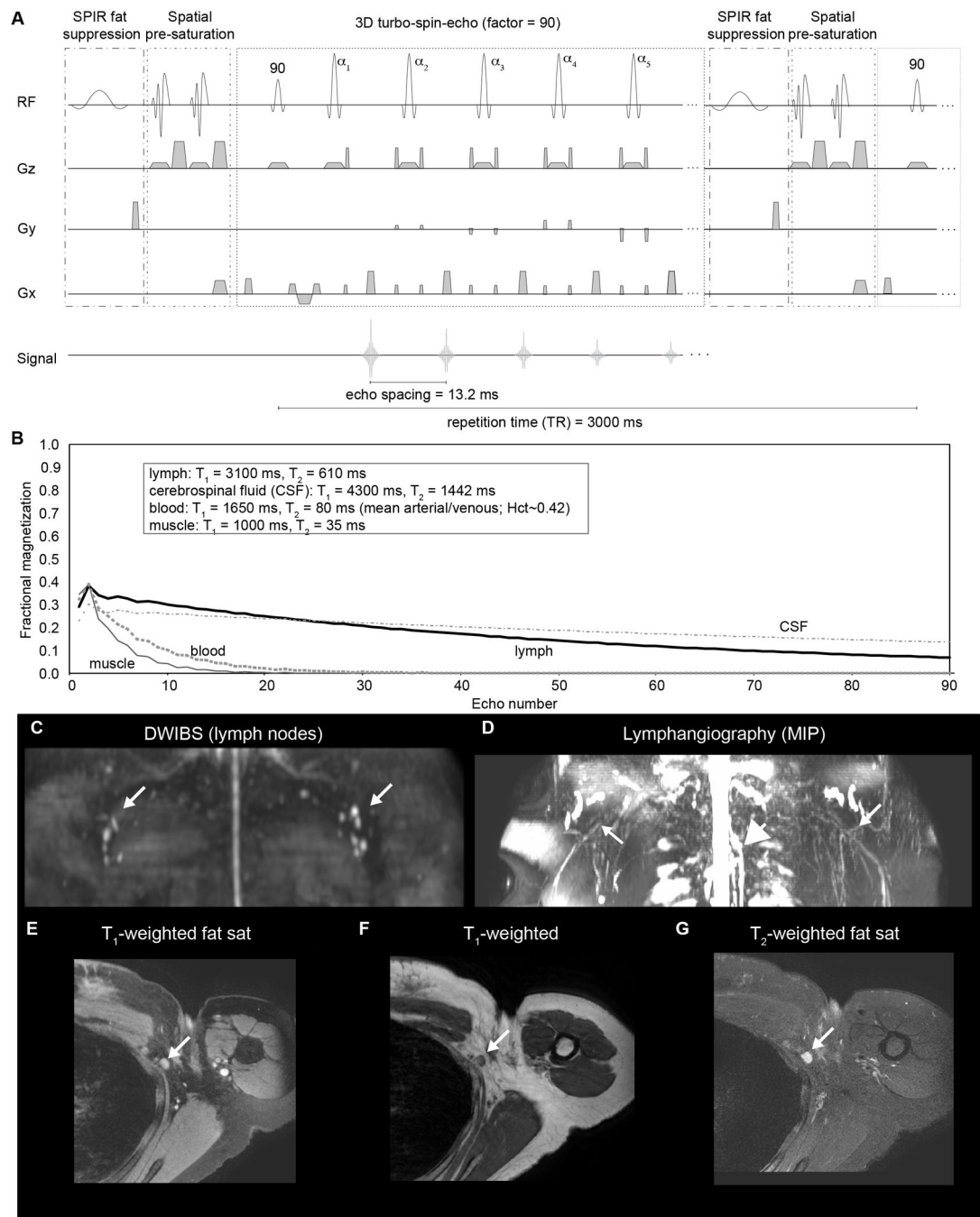
Figure 1.

(A) Relevant components of the proposed lymphangiography sequence, which consists of spectral presaturation with inversion recovery (SPIR) and spatially-selective presaturation pulses for fat and inflow suppression, respectively. Preparation is followed by a long turbo-spin-echo (TSE) readout (TSE-factor = 90; echo spacing = 13.2 ms; effective echo time = 600 ms). (B) These parameters lead to a fast decay of blood and muscle signal over the readout, yet a slower decay of lymphatic and CSF magnetization due to longer T_2 and lower velocity of these species. For a health control volunteer, (C) structural imaging of lymphatics

are displayed as the maximum intensity projection (MIP) from diffusion-weighted-imaging-with-background suppression (DWIBS) and (D) the lymphangiography sequence, showing the thoracic duct (large central white arrow) and convergence of apparent lymphatic vessels near the axillary lymph nodes (white arrows). Note that since lymphatic node T_1 and T_2 are substantially lower than lymphatic fluid T_1 and T_2, the lymphatic nodes are not clearly visible in the lymphangiography sequence. (E-G) High spatial resolution structural imaging at the site of an axillary lymphatic node (white arrow).
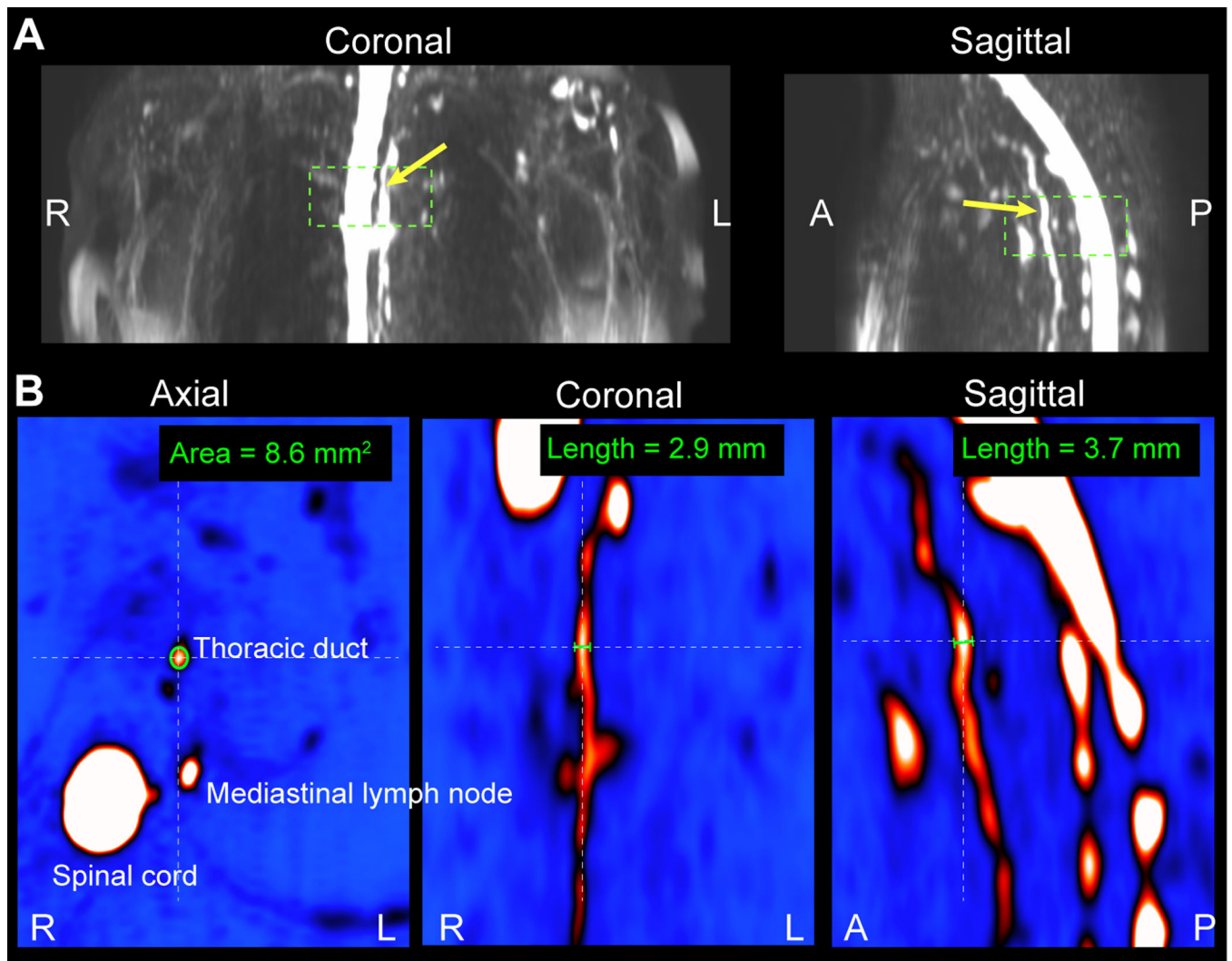
Figure 2.
Lymphatic vessel cross-sectional area measurement procedure. (A) Orthogonal representations of lymphangiography MIPs are generated to locate the lymphatic vessel of interest. This example is performed on the thoracic duct (yellow arrow) which is located anterior to the spinal cord. (B) The cross-sectional area is measured on magnified versions of the magnitude images themselves where vessel size can be confirmed in all three imaging planes.
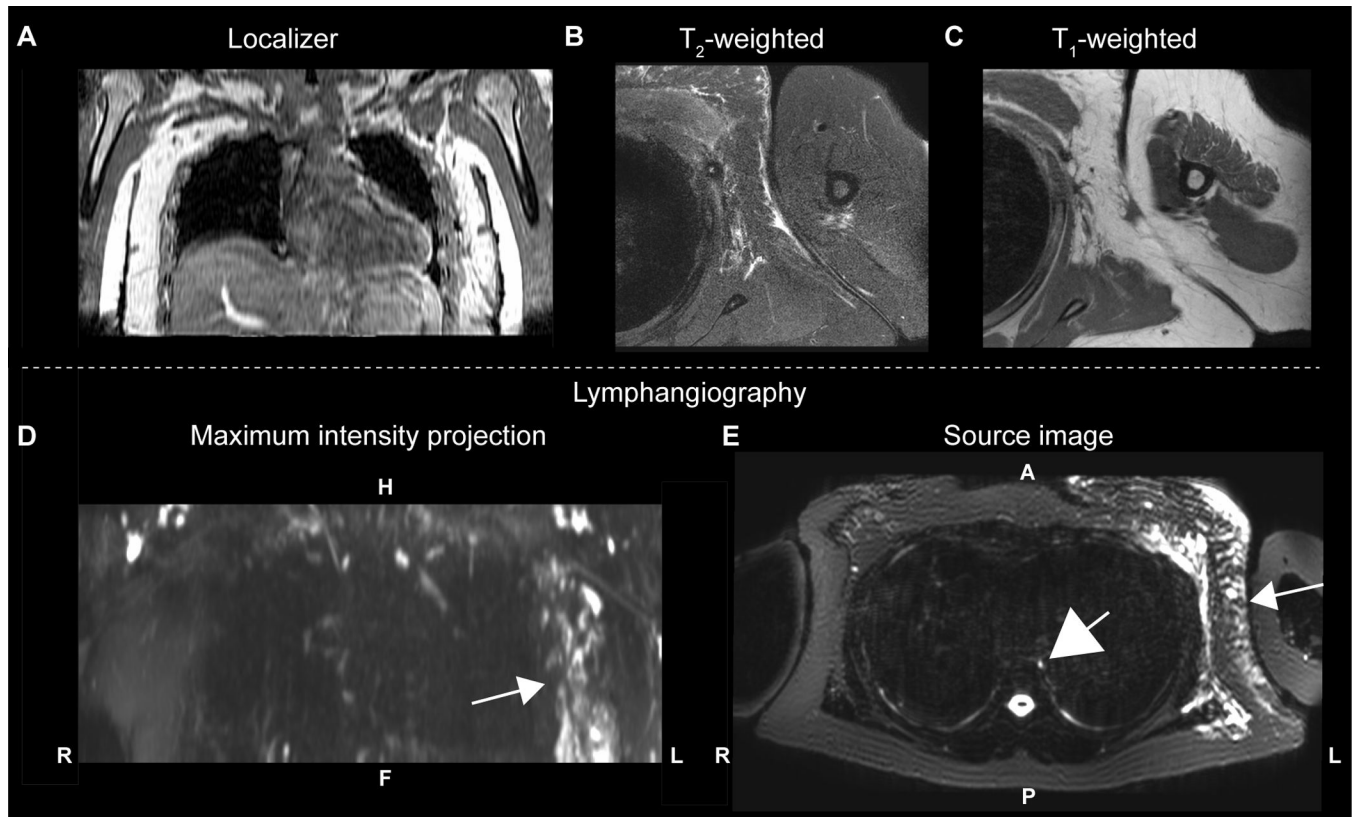
Figure 3.
A 53 year old female with left-sided Stage 1 BCRL (onset < 1 month) imaged at the end of radiation therapy and three months after 17 lymph nodes (all negative for carcinoma) were removed. (A) The T_1-weighted localizer shows the region imaged, along with (B) T_2-weighted and (C) T_1-weighted structural imaging of the involved side. Regions of subcutaneous edema are visible in the T_2-weighted scan. A (D) coronal MIP and (E) source image from the lymphangiography scan show contrast asymmetry between affected and contralateral quadrants (white arrows). The thoracic duct (E; large central white arrow) is also clearly visible. Compared with the subcutaneous edema seen in (B), the lymphatic vessels in (D-E) can be traced on continuous slices in a complex matrix of dilated tubes and channels.
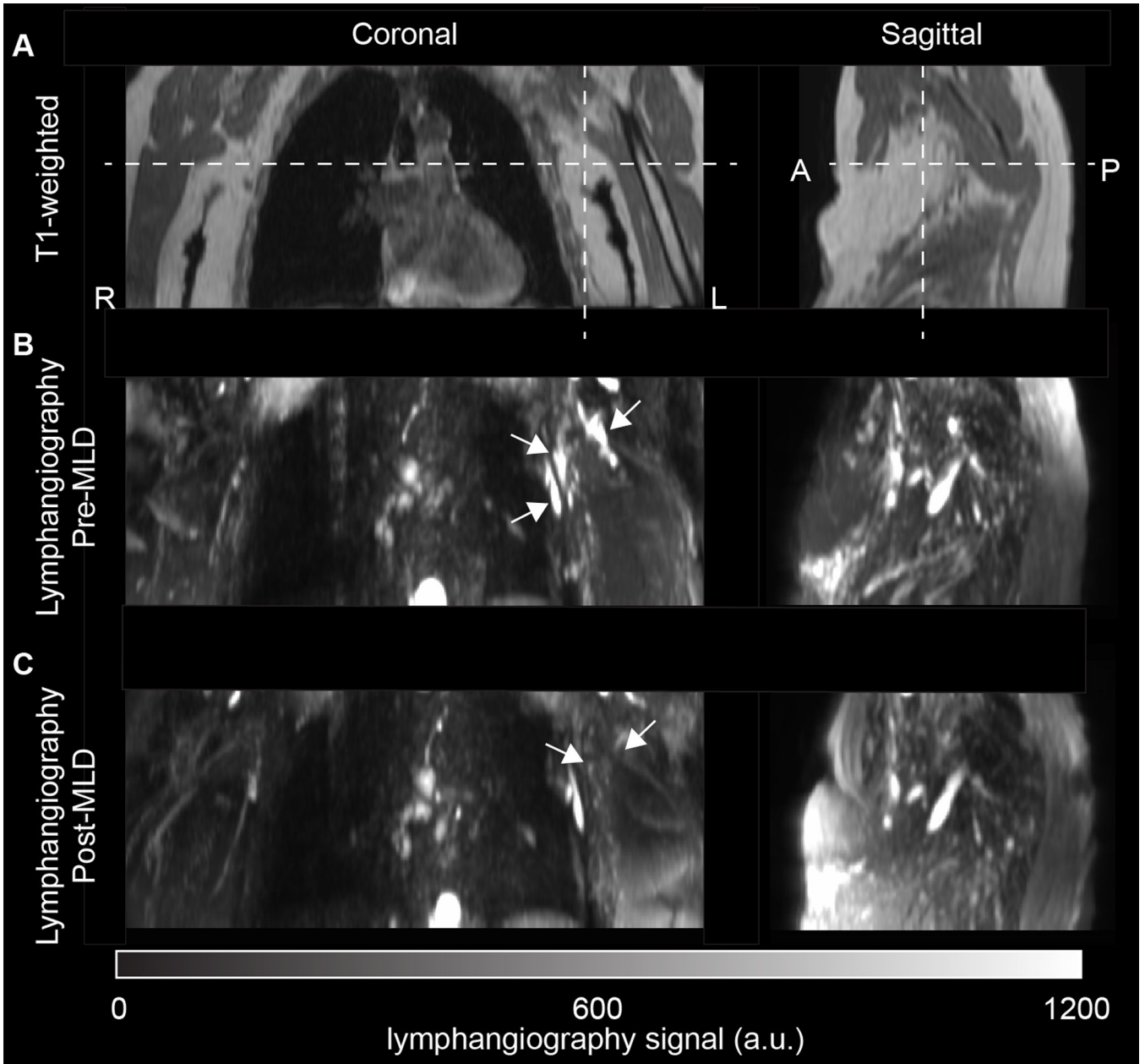
Figure 4.
Lymphangiograms pre (above) and post (below) manual lymphatic drainage (MLD) therapy for a 78 year old female with left-sided Stage 2 BCRL scanned three years after neoadjuvant chemotherapy, radiation, and removal of 14 lymph nodes (8 positive for carcinoma). The patient experienced reduced stiffness of her limb following a 50-minute session of MLD along with the therapist palpating reduction in fibrosis and induration of the skin along the left inner forearm, upper medial arm and lateral chest wall. The post-MLD findings indicate a reduction but not complete elimination of contrast consistent with lymph stasis (white arrows). Future MLD sessions could focus attention on rerouting the remaining congestion along the lateral chest wall to the ipsilateral lower quadrant. Reductions in contrast
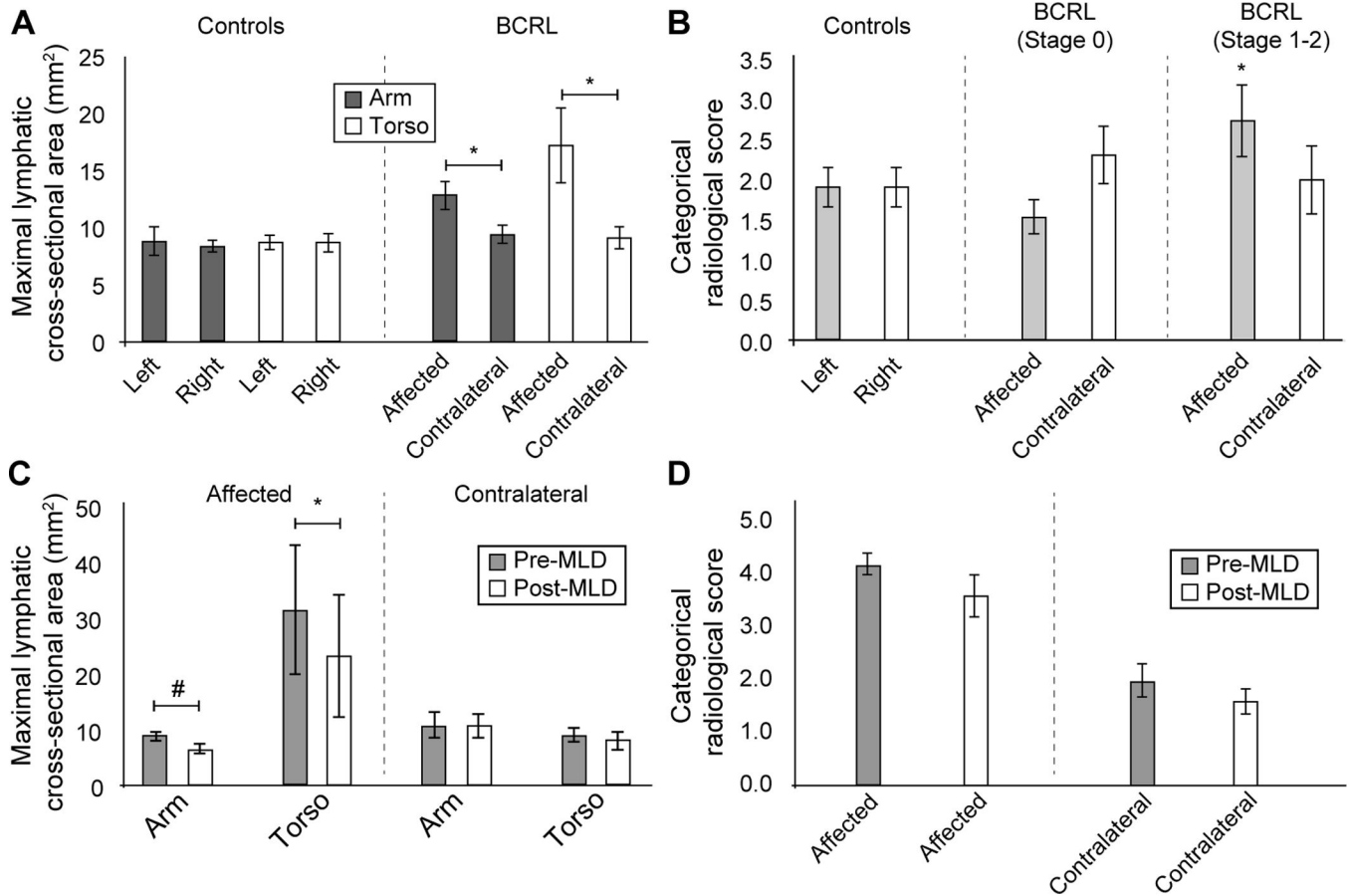
consistent with mobilization of lymphatic fluid are depicted by white arrows in (B-C) on the affected side.

Figure 5.
Summary of primary study findings. (A) Maximal lymphatic cross-sectional area did not differ significantly between left and right sides in controls, but was significantly elevated in the affected relative to contralateral side of patients. This was found both for arm and torso vessels and for both symptomatic (Stages 1–2) and sub-clinical patients. (B) The categorical scoring system was less sensitive to lateralizing disease. Neither left vs. right scores in controls, nor affected vs. contralateral scores in all patients, were significantly different. When only symptomatic patients were considered however, the scores in the affected side were significantly elevated relative to control scores. (C) In the subgroup of patients scanned before and after MLD, maximal lymphatic cross-sectional area was observed to reduce on the affected side only; this change was significant in the torso region and just beyond significance criteria in the arm region. (D) The categorical score changes pre- vs. post-MLD were not significant, however the effect sizes for the reductions were large on both the affected (Cohen's d=0.81) and contralateral (Cohen's d=0.63) side. * two-sided p<0.05; # one-sided p<0.05. Values summarized are mean ± one standard error of the mean. Standard deviations are summarized as well in Table 2.

Table 1

Proposed radiological scoring system, with increasing scores consistent with physiological changes occurring in more advanced stages of lymphedema.

Categorical score	Description
(unscored)	Images of unacceptable diagnostic quality
1	No lymphatic vessels or scant, thin lymphatic vessels discernable
2	Thin linear lymphatic vessels discernable without heterogeneity
3	Engorged linear lymphatic vessels discernable with signal heterogeneity
4	Engorged linear and tortuous lymphatic vessels discernable with or without signal heterogeneity (cloud pattern)
5	Engorged or non-engorged lymphatic vessels discernable with varying diameter with signal heterogeneity (beading pattern)

Table 2

Control (above) and patient (below) demographics, maximal lymphatic vessel cross-sectional areas, and radiological scores. All patient values are shown, along with those for only sub-clinical patients (Stage 0) and symptomatic patients (Stages 1 and 2). Values shown are mean ± one standard deviation.

	N	Age [range] (years)	Handedness (% right)	Nodes removed (number)	Left area (mm²) Torso	Right area (mm²) Torso	Left area (mm²) Arm	Right area (mm²) Arm	Left Score	Right Score
Controls	11	50 [33–68]	100	0.0±0.0	8.7±2.1	8.7±2.8	8.8±4.2	8.4±1.6	1.9±0.8	1.9±0.8
	N	Age [range] (yrs)	Affected side (% right)	Nodes removed (number)	Affected vessel area (mm²) Torso	Contralateral vessel area (mm²) Torso	Affected vessel area (mm²) Arm	Contralateral vessel area (mm²) Arm	Affected Score	Contralateral Score
All Patients	25	62 [44–80]	26.9	8.2±7.4	17.2±15.6	9.1±4.6	12.9±6.3	9.4±3.9	2.1±1.3	2.2±1.3
Patients (Stage 0)	14	61 [44–74]	14.3	4.1±2.8	12.8±6.5	9.0±5.1	12.1±5.8	8.8±4.3	1.5±0.8	2.3±1.3
Patients (Stages 1–2)	11	63 [46–80]	41.2	13.5±8.2	22.9±21.8	9.3±4.1	13.9±7.0	10.3±3.4	2.7±1.5	2.0±1.4